PCCP

PAPER

View Article Online
View Journal | View Issue

Cite this: *Phys. Chem. Chem. Phys.*, 2024, **26**, 24941

Insight into ion dynamics in a $NaClO_4$-doped polycaprolactone solid polymer electrolyte for solid state batteries†

Supriya K. Shetty, [a] Ismayil, *[a] Pradeep Nayak, [a] Y. N. Sudhakar, [b] Kuldeep Mishra, [c] Shahid Bashir [d] and Ramesh Subramaniam [e]

Received 2nd April 2024,
Accepted 9th September 2024

DOI: 10.1039/d4cp01360c

rsc.li/pccp

Employing low T_g polymers has fundamental limitations in providing the desirable ionic conductivity at ambient temperature due to the freezing of chain dynamics. The stiffening of polymer chains and the formation of highly ordered systems due to the crosslinks have influenced the ionic conductivity. Ionic conductivity of 1.02×10^{-5} S cm^{-1} was attained for the system that presented a quantum mechanical tunnelling mode of ion transport. A Na-ion transference number of 0.31 was achieved for 30 wt% of $NaClO_4$ salt in a polycaprolactone (PCL) matrix with an electrochemical stability window of 3.6 V at 25 °C. High crystallinity and limited availability of free Na^+ ions in the electrolyte have resulted in lower ionic conductivity. PCL–$NaClO_4$ exhibited brilliant thermal stability and mechanical properties. The influence of cathode materials MnO_2, V_2O_5 and I_2 on the discharge characteristics of an electrochemical cell in the configuration cathode |(70 wt%)PCL–$NaClO_4$(30 wt%)|Na has been studied.

Introduction

Solid polymer electrolytes (SPEs) play a crucial role in the development of high-performance energy storage systems (ESSs). SPEs are a promising candidate in primary/secondary batteries, hybrid/pseudo capacitors, and fuel cells. A fundamental understanding of the relationship between the chemical structure (ion–dipole interaction) and the ion transport properties in SPEs is necessary to achieve desirable ionic conductivity and electrochemical stability window (ESW), parameters that decide the life cycle of the battery.[1,2] The factors influencing the ion transport mechanism in polymer electrolytes require a deeper understanding for the development of next-generation ESSs based on SPEs. Polymer electrolytes are one of the alternatives to the liquid electrolytes for Na-ion batteries, bearing the advantages of ease of processability and cost-effectiveness. They have moderate ionic conductivity and poor interfacial contact compared to gel and liquid electrolytes.[3] One of the strategies used to achieve high ion-conducting polymer electrolytes is choosing a polymer host with low T_g.[4] According to the fundamental theories proposed, the low glass transition temperature (T_g) polymers are preferred as the polymer host in SPEs to achieve high ionic conductivity at ambient temperature. The coupling of segmental motions of polymer chains with ion transport above T_g creates a disordered environment for the conduction of ions. The hopping mechanism of ions is accompanied by the segmental motion of the polymer chain resulting in a faster ion-conduction mechanism, thus enhancing ionic conductivity. The operating temperature range of the battery for military applications is −50 to 80 °C,[5] and therefore the polymer with T_g lying below the range of working temperatures is preferred for battery applications. Polycaprolactone (PCL) is a hydrophobic, semicrystalline, ester-based biodegradable polymer with T_g = −60 °C that promotes ion transport of cations that is complexed with ester oxygen *via* segmental relaxation of the polymer chains. PCL polymer has been explored as the matrix in proton (H^+)[6] and lithium (Li^+)[7,8] ion conducting SPEs and henceforth in this work we have inspected it in a (Na^+) ion conducting SPE. The conductivity of the polymer electrolyte gets affected by the T_g, density of the coordination site, salt concentration and temperature.[9] Various theoretical models have been proposed to understand the ion conduction mechanism in SPEs but

[a] *Department of Physics, Manipal Institute of Technology, Manipal Academy of Higher Education, Manipal 576104, Karnataka, India. E-mail: ismayil.mit@manipal.edu, ismayil.486@gmail.com*
[b] *Department of Chemistry, Manipal Institute of Technology, Manipal Academy of Higher Education, Manipal 576104, Karnataka, India*
[c] *Symbiosis Institute of Technology, Symbiosis International (Deemed University), Pune, Maharashtra 412115, India*
[d] *Higher Institution Centre of Excellence (HICoE), UM Power Energy Dedicated Advanced Centre (UMPEDAC), Level 4, Wisma R&D, Universiti Malaya, Jalan Pantai Baharu, 59990 Kuala Lumpur, Malaysia*
[e] *Centre for Ionics Universiti Malaya, Department of Physics, Faculty of Science, Universiti Malaya, 50603 Kuala Lumpur, Malaysia*

† Electronic supplementary information (ESI) available. See DOI: https://doi.org/10.1039/d4cp01360c

never touched upon the influence of macroscopic structure on the same. Here, a Na^+ ion conducting SPE based on PCL polymer doped with sodium perchlorate salt was synthesized. The impact of cations and anions on the electrochemical and physico-chemical properties, along with the ion transport mechanism has been reported. A solid-state battery was fabricated with different cathode materials in the configuration cathode |(70 wt%)PCL–$NaClO_4$(30 wt%)|Na to study their influence on the discharge characteristics as well as the energy density and power density of the cell. Optimizing a cell for a specific application depends on the cathode material chosen.

Experimental

Materials, synthesis, and characterization

Poly(ε-caprolactone) (PCL, M_n = 80 kDa), sodium perchlorate ($NaClO_4$) salt and tetrahydrofuran (THF) solvent were purchased from Sigma Aldrich. PCL and sodium perchlorate salt with different weight ratios as tabulated in Table 1 were dissolved in THF solvent stirred for 4 hours and cast on a glass Petri dish covered with perforated aluminum foil for slow evaporation of the solvent. The thickness of the samples was measured using Mitutoyo micrometre. Cathode materials iodine (I_2, molecular weight (MW) = 253.81 g mol^{-1}) and vanadium pentoxide (V_2O_5, MW = 181.88 g mol^{-1}) were supplied by Loba Chemie Pvt. Ltd. MnO_2 was supplied by Labogens fine chem. Graphite (C, 100-micron, MW-12.01 g mol^{-1}) was purchased from S. D. fine-Chem Pvt Ltd.

Fourier-transform infrared (FTIR) spectroscopy

FTIR spectroscopy of the films was recorded in the wavenumber region between 4000 and 400 cm^{-1} with a resolution of 4 cm^{-1} using an IRPrestige-21 FTIR (SHIMADZU) to understand the interaction between the ions and functional groups.

X-Ray diffraction (XRD)

To understand the influence of polymer–ion interaction on the microstructure properties especially on the crystallinity, XRD patterns were recorded using a 3rd generation Empyrean, Malvern Panalytical, the Netherlands with Cu-Kα (λ = 0.154 nm) in the 2θ range between 5° and 90°.

Table 1 Composition of the samples and their designation

PCL + $NaClO_4$			
PCL (g)	$NaClO_4$ (g)	Designation	Thickness (mm)
2	0	LP-0	0.071
1.9	0.1	LP-5	0.057
1.8	0.2	LP-10	0.058
1.7	0.3	LP-15	0.088
1.6	0.4	LP-20	0.107
1.5	0.5	LP-25	0.087
1.4	0.6	LP-30	0.083

Differential scanning calorimetry (DSC)

To investigate the influence of doping on glass transition temperature DSC traces were registered on a TA instrument DSC Q2000. Samples of about 5 mg are heated from RT to 100 °C and isothermally held for a few minutes, cooled down to −100 °C followed by heating from −100 °C to 100 °C all at the rate of 10 °C min^{-1}. T_g is taken as the midpoint of the heat capacity change in the second heating.

Thermogravimetric analysis (TGA)

TGA/DTG was carried out to determine the thermal stability of the prepared SPE. The measurement was performed using an SDT Q600 V20.9 build 20 instrument. A sample of approximately 5 mg weight was placed on a platinum crucible. The platinum crucible was inserted into the enclosed machine chamber and heated at a scan rate of 10 °C min^{-1} from 20 °C to 500 °C with nitrogen as a purge gas flowing at 80 mL min^{-1}.

Electrochemical impedance spectroscopy measurements

The ionic conductivity was estimated in the frequency range 50 Hz to 1 MHz by recording impedance (Z), phase angle (PH), capacitance (C_p), and dissipation factor (D) from room temperature to 60 °C using aHIOKI 3532-50 LCR HiTESTER.

Transference number and DC polarization

The sodium ion transference number (T_{Na^+}) for the highest conducting sample was determined by sandwiching the sample between the sodium amalgam in the Swagelok cell in the symmetric cell configuration Na–Hg|LP30|Na–Hg. The setup was polarized by a constant DC potential of 10 mV until a steady current was obtained. The transference number was obtained using the relation $T_{Na^+} = I_{ss}/I_o$, where I_o and I_{ss} are initial and steady-state currents, respectively. The DC polarization curve in the configuration SS|LP30|SS was registered using the Keithley source meter 2636B to study the motion of ions in the presence of a dc biasing voltage of 10 mV.

Linear sweep voltammetry (LSV) and cyclic voltammetry (CV)

A Swagelok cell was used to evaluate the electrochemical stability window of the highest conducting sample in the configuration Na–Hg|LP30|SS at the sweeping rate of 100 mV s^{-1} from 2 to 5 V (*vs.* Na^+/Na). The CV was performed between −1 to +1 V at 5 mV s^{-1} with two electrode systems using a CH600E potentiostat.

Dynamic mechanical analysis (DMA)

Tensile tests were carried out using the Instron, model using a rectangular shape specimen with a gauge length of 50 mm and

width of 25 mm and tested at the crosshead speed of 0.1 mm min^{-1} following ASTM standard method D882.[10] Prior to the test, the samples were maintained at a relative humidity of 55% in a desiccator containing a saturated solution of NaBr for 24 h.

Fabrication of the primary battery

The cell has been constructed using the highest conducting sample as the separator cum electrolyte with three different cathode/active materials: MnO_2 (manganese dioxide), V_2O_5 (vanadium pentoxide) and I_2 (iodide) to study their influence on the energy density and power density. Na metal of diameter 12 mm and thickness 2 mm is incorporated as the anode. In the preparation of the cathode material, graphite (C) is used for electron conduction. A uniform mixture of electrode materials in the ratio (3 : 1 : 1) of (active material : C : SPE) was prepared by grinding them using a pestle and mortar for a few hours and then making a pellet of diameter 13 mm under 5-ton pressure using a pellet pressing machine. The electrolyte was sandwiched between sodium metal and cathode material in the Swagelok cell configuration to study the characteristics of a battery using an OWON XDM2041 digital multimeter instrument.

Results and discussion

FTIR studies

FTIR spectra of the PCL, $NaClO_4$ and PCL–$NaClO_4$ complex system and peaks corresponding to various vibrational bands are depicted in Fig. 1(a). PCL shares carbonyl (C═O) and ester C–O–R active functional groups[11] and henceforth prominent variation is observed in the corresponding region. The carbonyl group (C═O) available in the PCL polymers has a strong electron donor nature and is therefore very sensitive toward the formation of bonds with Na^+ ions resulting in the formation of a new broad peak at ~1637 cm^{-1}(ref. 12 and 13) as observed in Fig. 1(b). The intensity of the new peak formed at 1637 cm^{-1} increases with the increase in salt concentration. Polymer–ion interaction can bring about a shift in the vibrational modes, peak intensity, and band-broadening.[14] Two prominent interactions have been observed in the PCL–$NaClO_4$ electrolyte system, (C═O···Na^+) interaction and the other prominent change in the band structure was observed in the wavenumber region 1200–1000 cm^{-1}. FTIR deconvolution was carried out in the region 1200–1000 cm^{-1} using Fityk software as depicted in Fig. S1 (ESI†) and from the deconvoluted graph, changes in band structure are evident. The interaction (C═O···Na^+) also affects other vibrational modes of the polymer. The interaction of Na^+ ions with the carbonyl and with the oxygen C–O–R groups has resulted in a change in bond length corresponding to C–O–R[11] and thus resulted in the shape change of the bands in the 1200–1000 cm^{-1} region. In this region, coupled modes of vibration such as asymmetric stretching of (C–O–C) at ~1163 cm^{-1}, asymmetric and symmetric stretching of C–O at 1163 cm^{-1} and 1108 cm^{-1}, respectively, C–C and C–O stretching vibrations at 1157 cm^{-1} and C–O stretching and CH_2 rocking[15] at 1043 cm^{-1} takes place. In the deconvoluted spectra, the wavenumber [ϑ(C–O–C)] at ~1066 cm^{-1} exhibited broadening and the band [ϑ_s(O–C)][15] at ~1107 cm^{-1} eventually disappeared with an increase in salt

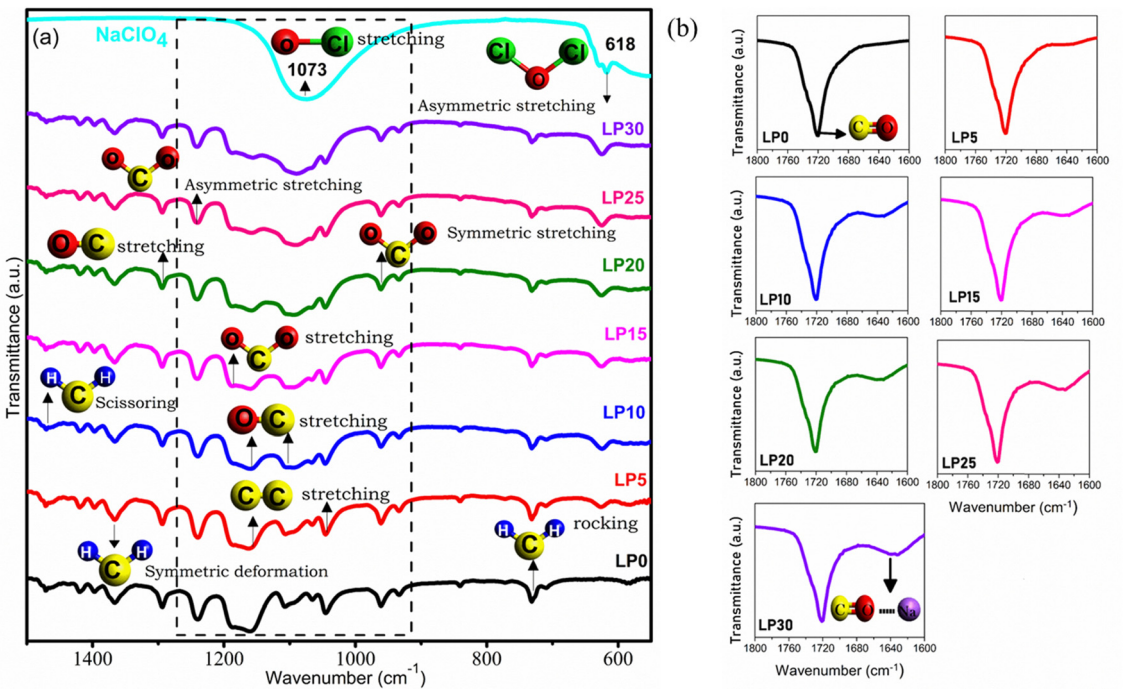

Fig. 1 FTIR spectra of PCL, $NaClO_4$ and $NaClO_4$ complexed PCL solid polymer electrolyte films (a). Formation of a new peak in the wavenumber region 1600–1800 cm^{-1} due to C═O···Na^+ interaction (b).

concentration due to the combined effect of $Na^+\cdots O$–C and C═O$\cdots Na^+$ interaction.[16]

X-Ray diffraction studies

The XRD pattern of the PCL polymer exhibits a semicrystalline nature with peaks at $2\theta = 21.4^\circ$, 22.1°, and 23.8° associated with (110), (111), and (200) orientations corresponding to the orthorhombic crystal structure, as shown in Fig. 2.[17] The shift in the peaks reveals the interaction of Na^+ with the carbonyl group and resulted in cross-links between the PCL chains influencing the crystallinity. Using Fityk software, XRD data has been fitted by employing the Gaussian function, and the percentage of crystallinity is evaluated using the equation $\chi_c = \frac{A_c}{A_a + A_c} \times 100\%$. Here A_c is the area of the crystalline region, A_a is the area of the amorphous region and c is the percentage of crystallinity. Gaussian fit has resulted in three crystalline peaks and one broad amorphous halo centered at $2\theta = 21^\circ$,[18] whose intensity decreased with an increase in salt concentration with a high peak-to-background ratio, thus increasing crystallinity as observed in Fig. 3. The variation in the percentage of crystallinity as a function of salt concentration is shown in Fig. 3. The increase in crystallinity with salt concentration will affect the relaxation of the polymer chain, thus influencing the ion conduction mechanism.

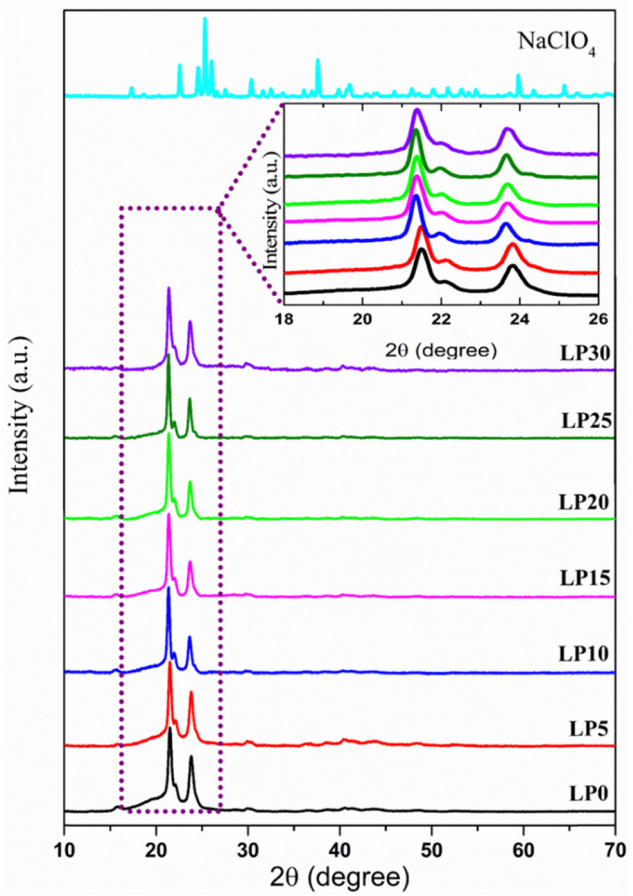

Fig. 2 XRD pattern of the PCL, $NaClO_4$, and PCL–$NaClO_4$ electrolyte system.

Differential scanning calorimetry studies

DSC measurements have been carried out to understand the influence of doping on the segmental mobility of the polymer chains. Fig. 4(a) exhibits the DSC thermogram for different weight percentages of $NaClO_4$ salt with a zoomed-in image at the phase transition as shown in Fig. 4(b). An increase in T_g is the result of an increase in cross-link points –C═O$\cdots Na^+\cdots$O═C as shown in Fig. 4(c). The strength of interaction of the carbonyl group with Na^+ will determine its transport number.[19] The transient crosslink restricts the local chain kinetics and its rate, thus having an influence on the mobility of ions. A non-uniform variation of T_g with salt concentration has been observed attributed to the diverse interaction of ions with different segments of the polymer chains. These interactions influence the packing and mobility of the polymer chains in a non-uniform manner, leading to localised variations in T_g. The sharp endothermic melting peak (T_m) corresponds to the melting of the crystalline phase. The crystallization ability of PCL–$NaClO_4$ systems was strengthened with the increase in salt concentration resulting in the enhancement of long-range ordering. Disappearing melting peaks are not observed, suggesting no reduction in crystallinity. The crystallinity of the polymer/SPE restricts the molecular movement of polymer chains and thus resulted in an increase in T_g. The average free volume decreased as there was an increase in T_g due to the formation of transient crosslinks due to the interaction of Na^+ with the ester oxygen. The chemical nature of the ion and polymer will influence the segmental mobility of the polymer chains (T_g)[20] and therefore choosing the appropriate polymer and salt is necessary. The relationship between T_g and T_m roughly follows $T_g = 0.7T_m$, and the accepted ratio of T_g/T_m lies between 0.5 to 0.8.[21]

Thermogravimetric analysis (TGA)

Thermograms of PCL and LP30 samples are depicted in Fig. 5(a). Thermal degradation of PCL started around 325 °C, with a sharp peak at 402 °C[22] and degraded completely at 425 °C without any residue (Fig. 5(b)). LP30 sample degradation begins around 231 °C due to residual THF followed by the main degradation of the polymer. The thermal stability value for PCL is approximately 100 °C higher than that of the LP30 system, implying that the salt in the LP30 sample has significantly lowered onset temperature of the main degradation process. The rate of thermal degradation is rapid in PCL compared to the LP30 system. Thermal degradation of PCL involves scissoring of ester linkages producing CO_2 gas, water and carboxyl acid that have resulted in shoulder peaks observed at 348 °C and 391 °C, which implies thermal degradation involving different mechanisms followed by depolymerization. The main degradation peak of PCL at 402 °C is the result of depolymerization with volatile gases such as CO_2 and H_2O. The thermal activation energy (E) was evaluated from the Coats Redfern

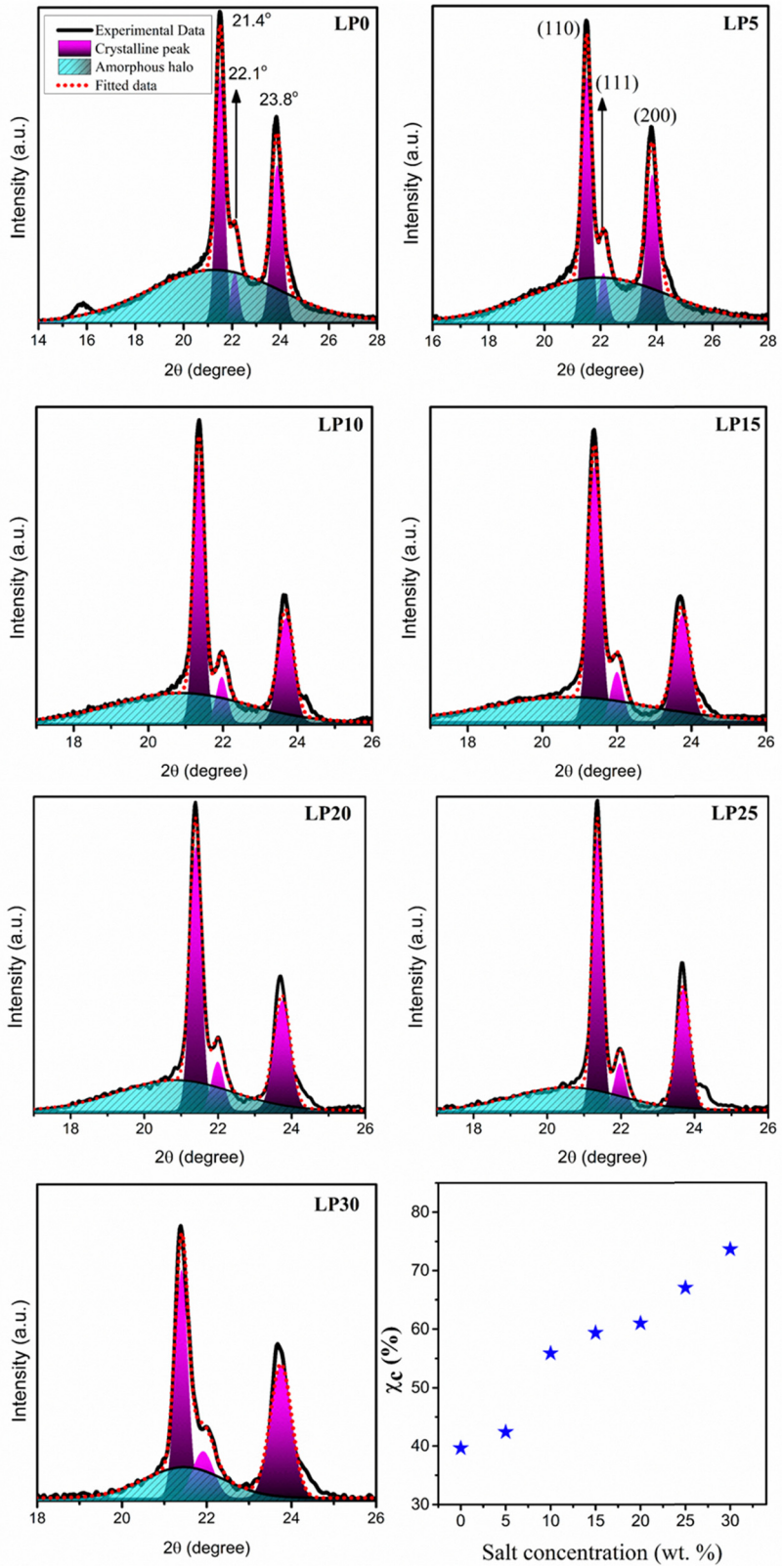

Fig. 3 Deconvoluted XRD pattern of the PCL and PCL–$NaClO_4$ SPE and variation of the crystallinity with salt concentration.

integral equation (Coats & Redfern, 1964)[23] as shown in Fig. 5(c) and (d) for samples LP0 and LP30, respectively. A decrease in thermal activation energy for the LP30 electrolyte system compared to PCL indicates the reduction in thermal stability and it indicates the influence of doping on the thermal stability of the SPE. This change depends on the type of salt

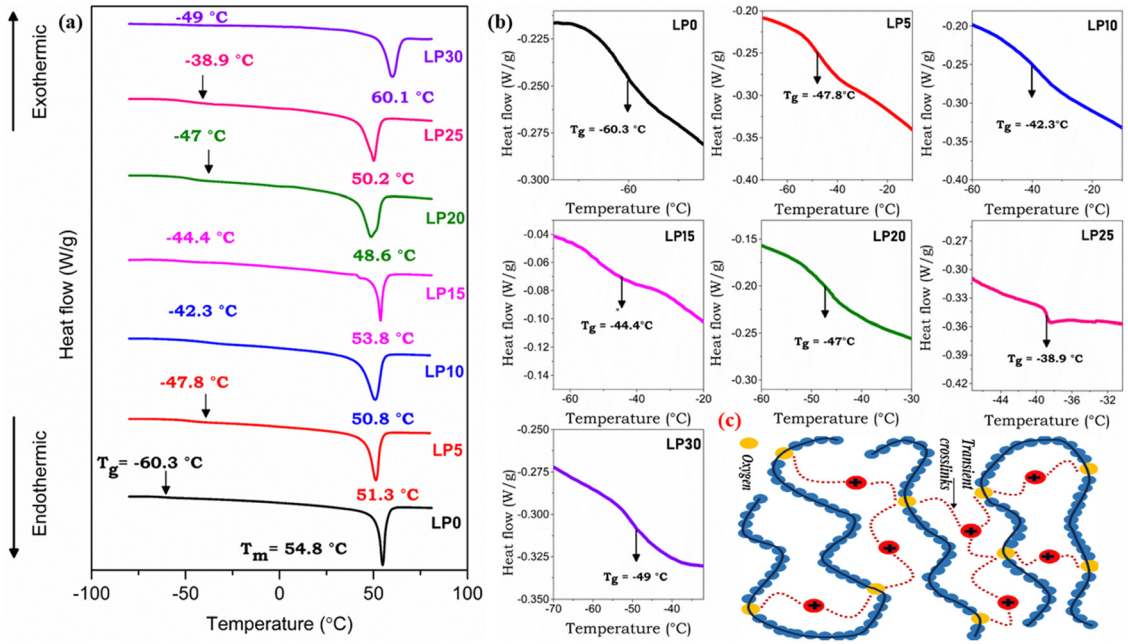

Fig. 4 DSC thermograph of the PCL and PCL–$NaClO_4$ polymer electrolyte system (a). Zoomed-in image at the phase transition (b). Schematic representation of transient crosslinks (c).

doped in the polymer matrix and the type of interaction between the polymer and the ions.

AC conductivity studies

AC conductivity varies according to a universal power law (UPL) in the PCL–$NaClO_4$ system as per the equation,

$$\sigma(\omega) = \sigma_{dc} + A\omega^{s}, \quad (1)$$

where σ_{dc} is the frequency independent conductivity, A is the frequency exponent and s ($0 < s < 1$) characterizes the electrical conduction mechanism. The nature of the curve as shown in Fig. 6(a) can be explained as per the jump relaxation model/UPL (universal power law).[24] In this frequency window a low-frequency plateau region (σ_{dc}) is followed by a dispersion region ($A\omega^{s}$). The deviation of σ_{dc} at very low frequency signifies the electrode polarization and its prominence as salt concentration increases, indicating more ions at the electrode/electrolyte interface (fast ion migration). The hopping of ions from one coordinate site to another is responsible for both dc and ac conductivity. For the ions to hop to the newly favourable neighbouring unoccupied site there is a need for a potential minimum (W_m) to be formed at that site and its formation need not be instantaneous; therefore, there is the possibility of hopping back to the initial site. The chance of forward–backwards motion at a higher frequency due to a short period has resulted in a high-frequency dispersion region (short-range ion hopping). Fitting eqn (1) (as shown in Fig. 6(a) for LP25 sample) gives the parameters σ_{dc}, A and s. The ion conduction mechanism in the polymer electrolyte can be explained by different models based on the variation of s with temperature, such as quantum mechanical tunnelling (QMT) (where, s is temperature independent), correlated barrier hopping (CBH) (s decrease with increase in temperature), small polaron quantum mechanical tunnelling (SP) (s increases with temperature) and overlapping large polaron (OLP) (a decrease and then increase in s with temperature). The variation of exponent s with temperature is as shown in Fig. 6(c). s decreased with an increase in temperature for the LP15, LP20 and LP25 samples and thus the CBH model could describe the conduction mechanism in these samples. For the CBH model, the temperature and frequency dependence of s is expressed in eqn (2).[25]

$$s = \frac{1 - 6kT}{W_m - kT\ln(\omega\tau)} \quad (2)$$

where W_m is the maximum potential barrier height separating two energetically favourable sites (activation energy of polaron transfer/activation energy for hopping) at a frequency ω,[26] k is the Boltzmann constant, T is the absolute temperature and τ corresponds to the relaxation time for the ion to hop the barrier height, $\tau = \tau_o \exp(W_m/kT)$. Approximation of eqn (2)[25] gives, $s = \frac{1 - 6kT}{W_m}$. According to CBH, the charge carriers hop between the coordinate sites over a barrier of W_m, calculated from the slope of the line $(1 - s)$ *vs.* T. As per the QMT model, the value of the power exponent is nearly 0.8 and varies only with frequency and no correlation of the barrier height with hopping length exists.

$$s = 1 - \frac{4}{\ln(1/\omega\tau_0)} \quad (3)$$

The conductivity of the LP30 sample is found to be temperature independent. Since s is temperature independent as

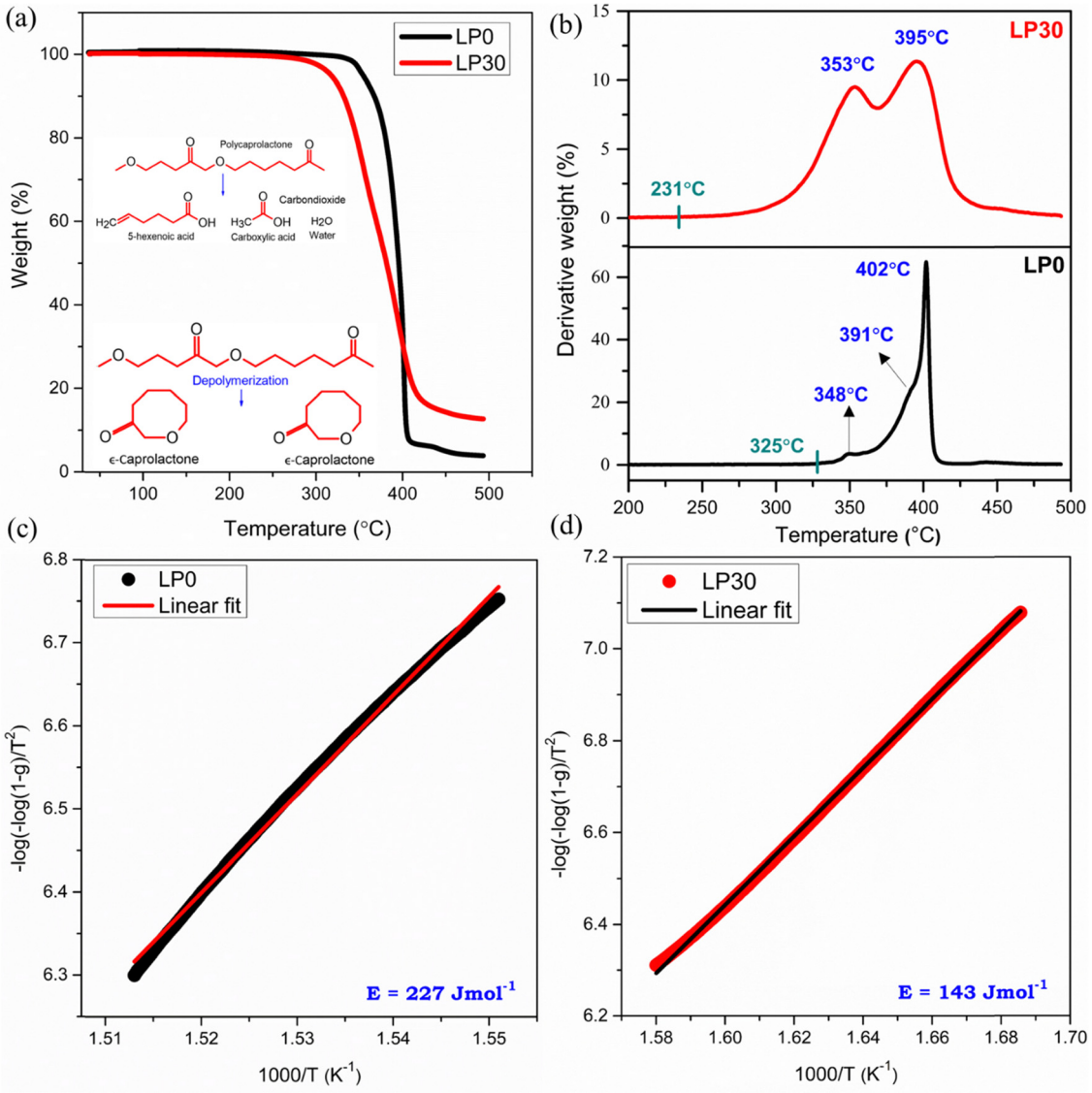

Fig. 5 TGA thermogram plot (a), DTG plot (b), and plot of $-\log\left[\frac{-\log(1-\gamma)}{T^2}\right]$ *vs.* $\frac{1000}{T}$ of the LP0 and LP30 samples (c) and (d), respectively.

shown in Fig. 6(c), it proves that the QMT process involves ion tunnels between the localized state near the Fermi level. As QMT is dependent on barrier separation (R) and independent of temperature, it was observed that ionic conductivity is independent of temperature for the LP30 sample, as shown in Fig. 6(b) [Table S1, ESI†]. In contrast, the hopping mechanism is temperature dependent and therefore an increase in conductivity with temperature is observed for other samples as observed in Fig. 6(b). The transportation of ions is influenced by the coordination environment, clearly observed in conductivity data (both CBH and QMT are observed). At low temperatures (region I), the dc conductivity is very small indicating the occurrence of a nearly constant loss (NCL) phenomenon usually observed in disordered systems that conduct ions. A crossover from NCL to region II is observed at higher temperatures where a sharp rise in σ_{dc} with temperature is observed, as shown in Fig. 6(b). Natesan *et al.*[27] demonstrated a crossover from the less sensitive temperature-independent conductivity region dependence to temperature-dependent conductivity for the first time in a polymer electrolyte system. NCL arises due to the slowing down of ionic motion in the coulombic cage either due to matrix molecules or ion–ion interaction.[28] The variation of conductivity shows two regions: region I ($T < 313$ K) and region II ($T > 313$ K) with two different activation energies both following Arrhenius behaviour concluding two different conduction mechanisms occurring and not because of any type of transition (glass transition/melting of crystalline phase) but due to differences in the physical environment experienced by ions while hopping.[29] At low temperatures, the mobile ions are assumed to be in a potential cage and the probability for ions to hop leaving behind the cage is low resulting in low ionic conductivity.[30,31] As the temperature increases, the universal dielectric response (UDR) dominates the NCL phenomenon by overcoming the potential cage resulting in a sharp increase in

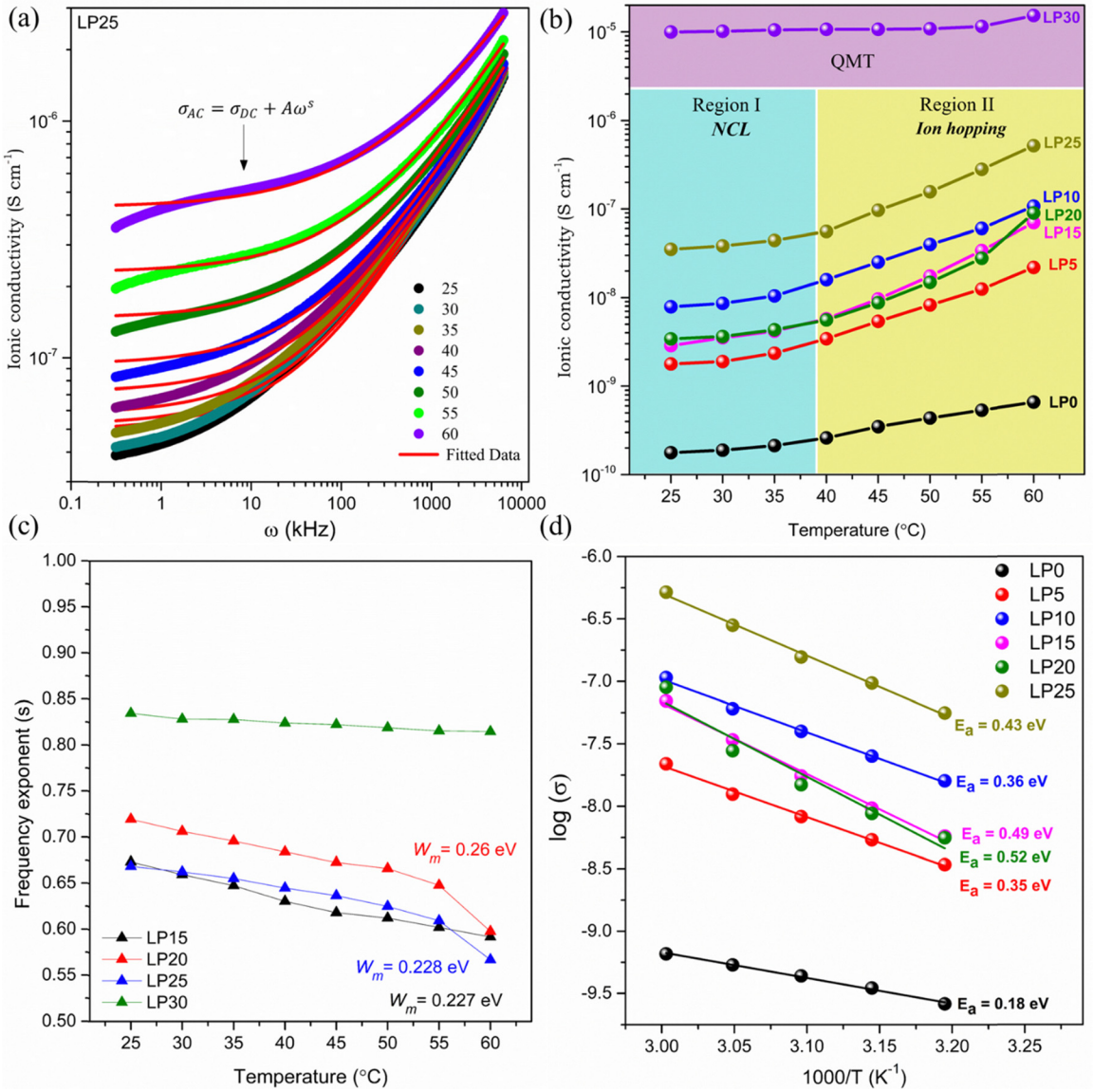

Fig. 6 AC conductivity of the spectra of the LP25 sample (a). Ionic conductivity plot at different temperatures (b). Variation of the frequency exponent with temperature (c) and activation energy (d).

ionic conductivity. Interchain, intrachain Na^+ hopping and coupling of segmental diffusion with Na^+ hopping can be the modes of ion transport in this electrolyte system as $T > T_g$. Coupling of the hopping mechanism with the segmental relaxation is possible in the amorphous phase, since the crystallinity has increased with salt concentration influencing the mode of ion transport and ionic conductivity. As the crystalline phase dominates in the PCL–$NaClO_4$ electrolyte system in comparison with the amorphous phase, ion transport in the crystalline phase takes place *via* ion hopping between the coordinate site along the polymer tunnels.[32] Thus, the temperature dependence of ionic conductivity follows an Arrhenius-type relation (4)[33]

$$\sigma(T) = A \exp\left[-\frac{E_a}{k_B(T)}\right] \quad (4)$$

where E_a is the activation energy, T is the absolute temperature, k_B is the Boltzmann constant and A is the pre-exponential factor. Since the crystalline phase of SPEs has increased, the ions must overcome the large energy barrier through the polymer dynamics, therefore giving a larger E_a as observed in Fig. 6(d). Decoupling of ion diffusion with the structural relaxation exhibits better ionic conductivity over the one having frozen chain kinetics and therefore has resulted in low ionic conductivity. The degree of crystallinity (χ_c) increased linearly with salt concentration concluding no direct correlation of σ_{dc} with χ_c. σ is obtained only up to 60 °C due to the presence of a melting peak, since the crystalline region melts above T_m and therefore has a significant influence on σ.[34] Nyquist plots of the pristine and PCL–$NaClO_4$ systems at 25 °C are depicted in Fig. S2 (ESI†), which illustrates high impedance to flow of ions. The tilted spike in the Nyquist plot increases with an increase

in salt concentration at 60 °C as shown in Fig. S3 (ESI†), indicating an increase in ion concentration at the electrolyte/electrode interface with increased salt content.

Transference number and transient ionic current

The coordination of Na^+ to the polymer chains will determine the Na^+ transference number (T_{Na^+}) and the weak coordination leads to high transference number. Thus, the functional group available in the polymer chains and the strength of the polymer–ion interaction will influence the cation transference number and thus the ionic conductivity. The coordination of Na^+ with the carbonyl oxygen of PCL has resulted in a transference number of about T_{Na^+} = 0.31 for the LP30 sample measured using the plot, as shown in Fig. 7(c). The mobility (μ) and diffusion coefficient (D) of ions of the LP30 sample have been evaluated from the following equations $\mu = \frac{eD}{k_B T}$ and $D = \frac{e(k_2 \varepsilon_r \varepsilon_0 A)^2}{\tau_2}$, by fitting the Nyquist plot using the following eqn (5) and (6)

$$Z' = \frac{R + R^2 k_1^{-1} \omega^{p_1} \cos\left(\frac{\pi p_1}{2}\right)}{1 + 2Rk_1^{-1}\omega^{p_1}\cos\left(\frac{\pi p_1}{2}\right) + R^2 k_1^{-2}\omega^{2p_1}} + \frac{\cos\left(\frac{\pi p_2}{2}\right)}{k_2^{-1}\omega^{p_2}} \quad (5)$$

$$Z'' = \frac{R^2 k_1^{-1} \omega^{p_1} \sin\left(\frac{\pi p_1}{2}\right)}{1 + 2Rk_1^{-1}\omega^{p_1}\cos\left(\frac{\pi p_1}{2}\right) + R^2 k_1^{-2}\omega^{2p_1}} + \frac{\sin\left(\frac{\pi p_2}{2}\right)}{k_2^{-1}\omega^{p_2}} \quad (6)$$

Parameter k_1^{-1} is the geometrical bulk capacitance related to k_2^{-1}, the electric double layer capacitance, p_2 is a skew parameter that controls the deviation of the tilted spike from the Z'-axis, and p_1 is the ratio of the angle between the diameter of the semicircle and Z''-axis. k_B is the Boltzmann constant, T is

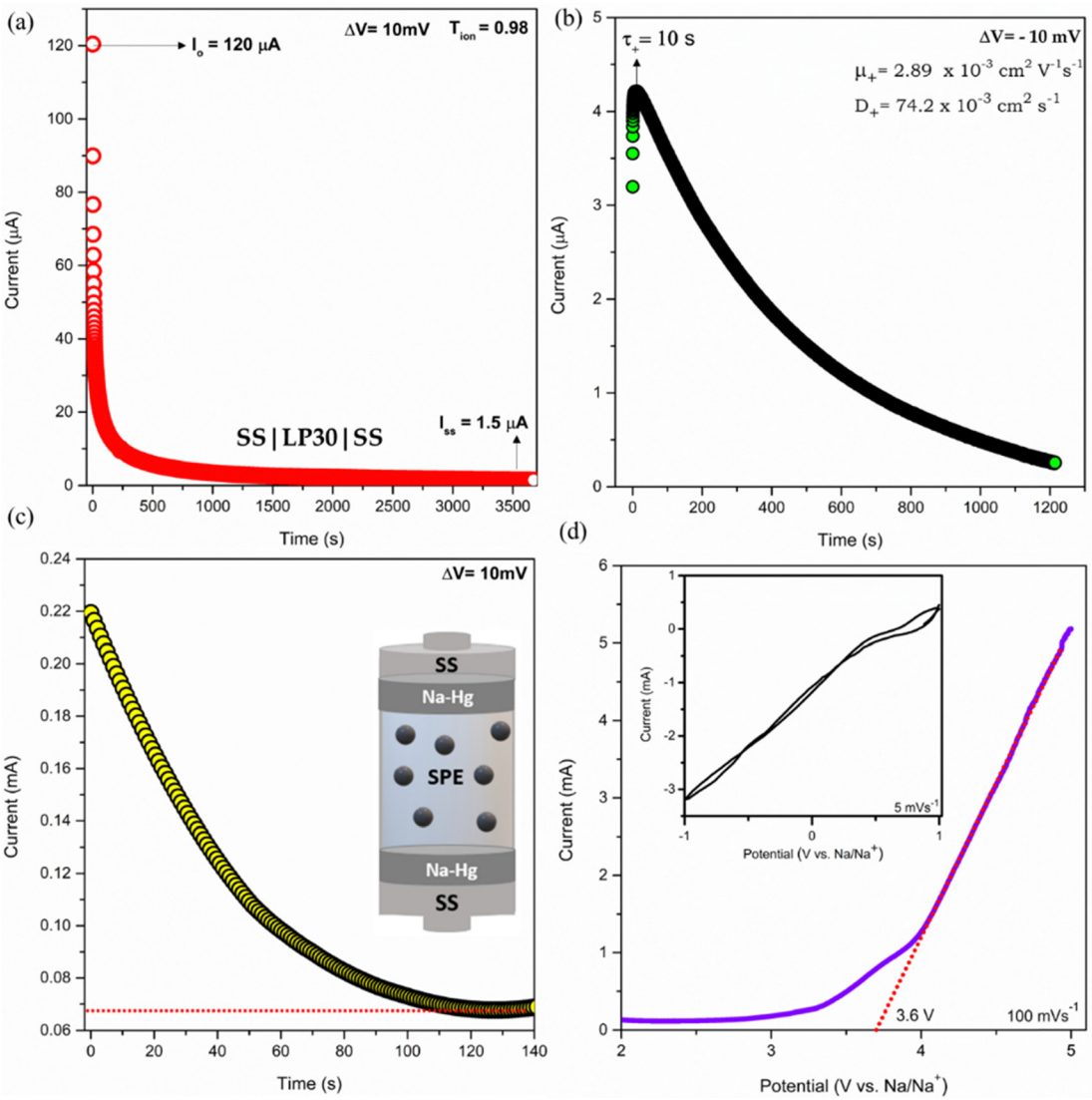

Fig. 7 Transient ionic current curve: (a) forward bias, (b) reverse bias, (c) current *vs.* time curve to determine the ion migration number of the cation and (d) LSV and CV curve for the LP30 sample.

absolute temperature, e is the electron charge, ε_r is the dielectric constant at high frequency (100 kHz), $\tau_2 = 1/\omega_2$ corresponding to the frequency at the minimum in the imaginary part of the impedance. The mobility and diffusion coefficient of the cation is evaluated using the relations $\mu_{Na^+} = \mu T_{Na^+}$ and $D_{Na^+} = DT_{Na^+}$, respectively. The mobility and diffusion coefficient of the anion is larger compared to that of the cation as observed in Table 2. The mobility of ions depends on the polymer matrix and the type of coordination site. The mobility of anions is higher than that of Na^+ ions, since the motion of cations is coupled with the Lewis base site of the polymer host and therefore in the dual ion conducting SPE, the cation transference number is lower than 0.5.[35] Na^+ cations have less mobility compared to the counter anion due to the highly coupled motion of sodium ions with Lewis base sites in the polymer matrix. Cations form strong ion–polymer bonds compared to anions and therefore result in faster anion diffusion. At lower salt concentrations, ion dissociation is easy due to the availability of coordination sites to dissociate the ions and the increase in the rigidity of the polymer chains and crystallinity will also influence the transference number. The transient ionic current plot in the forward and reversed polarization is shown in Fig. 7(a) and (b), respectively. Ionic conductivity is mainly due to ions as justified with $T_{ion} \approx 1$. The single peak observed in the transient ionic current plot corresponds to Na^+ ions, since the ionic radius of Na^+ (97 pm) is less than the ionic radius of ClO_4^- (240 pm). The mobility (μ_+) and diffusivity (D_+) of Na^+ were evaluated using the relation, $\mu_+ = \frac{t^2}{\tau_+ V}, D_+ = \frac{\mu_+ kT}{e}$, where t is the thickness of the film, $V = 10$ mV is the applied potential, and τ_+ is the time of flight of the Na^+ ion.[36] Reversibility of the Na^+/Na redox couple is observed in the inset plot of Fig. 7(d) and ESW of about 3.6 V was observed for the LP30 sample. The potential of sodium is −2.71 V. The typical batteries (Na-ion batteries) deliver cell voltages of 2.8 to 3.5 V.[37] One of the contributors (KM) has also reported a prototype sodium cell with a Na metal anode and phosphorous red cathode utilizing a gel polymer electrolyte system with an electrochemical stability window of ∼3.6 V.[38] We believe that, for the optimized electrolyte composition, layered transition metal oxides such as $NaCoO_2$, $NaFeO_2$, $NaNiO_2$, $NaCrO_2$, $NaVO_2$, *etc.* can be used as a cathode for cell fabrication.[37]

Table 2 Transference number, ionic conductivity, and transport parameters of ionic species of the LP30 sample

T_{Na^+}	$T_{ClO_4^-}$	σ_{Na^+} (S cm^{-1})	$\sigma_{ClO_4^-}$ (S cm^{-1})
0.31	0.67	3.2×10^{-6}	6.8×10^{-6}

Nyquist-fit			
μ (cm2 V^{-1} s^{-1})		D (cm^2 s^{-1})	
μ_{Na^+}	$\mu_{ClO_4^-}$	D_{Na^+}	$D_{ClO_4^-}$
0.35×10^{-6}	0.76×10^{-6}	9.08×10^{-9}	1.96×10^{-6}

Mechanical properties

The mechanical strength of SPE affects its performance in ESSs, the volume expansion of electrodes during charge/discharge cycles generates mechanical stress and the SPE must be in the position to withstand it. The safety and the reliability of the battery depend on the mechanical properties, by avoiding the short circuit.[39] The mechanical properties of the SPE depend on the percentage of crystalline phase, polymer structure and polymer–ion interaction, since the intermolecular forces get affected by the incorporation of salt thus disturbing the mechanical stiffness. The LP30 sample is flexible in comparison with the pristine one as observed from Fig. 8. Elastomer nature was observed due to the softness and flexibility of the PCL polymer and it therefore will be a good candidate in ESSs.

Primary battery fabrication

Practical applicability of the highest conducting sample (LP30) in primary batteries with different cathode materials was studied. Since the electrolyte is conducting Na^+ ions, sodium metal is chosen as the anode material. The discharge characteristics of the cells are shown in Fig. 9 and designated as below with the cell parameters tabulated in Table 3.

Cell 1: MnO_2 (3): C (1): LP30 (1) |LP30| Na

Cell 2: V_2O_5 (3): C (1): LP30 (1) |LP30| Na

Cell 3: I_2 (3): C (1): LP30 (1) |LP30| Na

A passivating layer is formed at the anode and cathode due to a side reaction that stops self-discharge and dissipates once connected to a load. Various factors are responsible for self-discharge, such as the electrodes forming a passivating layer in

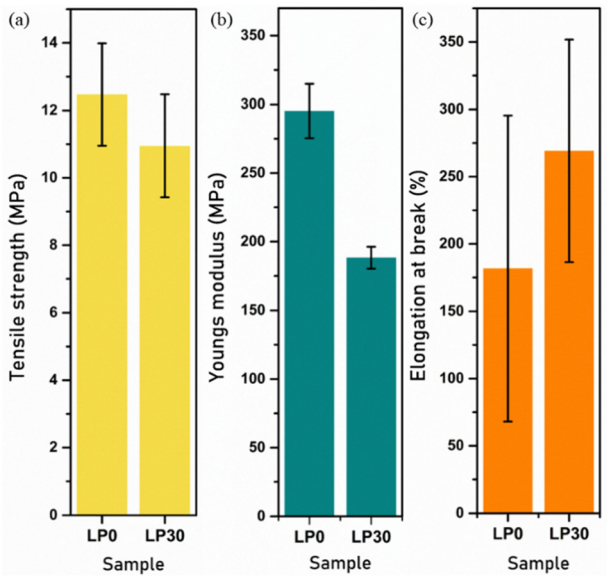

Fig. 8 Variation of the mechanical properties: (a) Tensile strength. (b) Youngs modulus. (c) Elongation at break of the LP0 and LP30 samples.

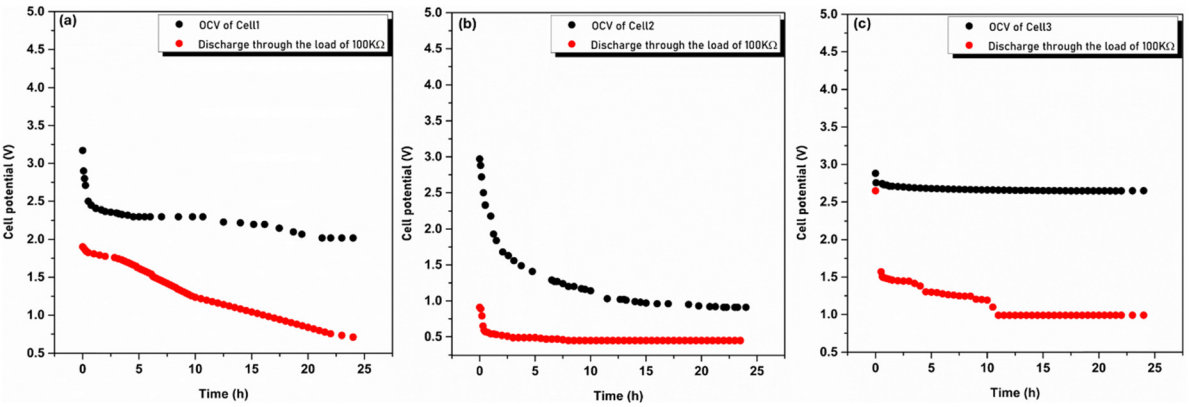

Fig. 9 Open circuit voltage and discharge characteristics of Cell 1 (a), Cell 2 (b) and Cell 3 (c).

Table 3 Comparison of cell parameters of solid-state batteries

	Measured values		
Cell parameters	Cell 1	Cell 2	Cell 3
Cell area (cm^2)	1.23	1.23	1.23
Weight of the cell (g)	1.46	1.1	0.97
Effective diameter of the cell (cm)	1.30	1.30	1.30
Thickness of the cell (cm)	0.5	0.5	0.4
Open circuit voltage (V)	3.17	2.97	2.88
Current drawn (mA)	0.1	0.18	0.35
Current density (mA cm^{-2})	0.08	0.14	0.28
Discharge time plateau region (h)	—	16	13
Discharge capacity (mA h g^{-1})	—	2.62	4.69
Energy density (mW h kg^{-1})	—	1178	4690
Power density (mW kg^{-1})	—	73.6	360

contact with air and the electrolyte, and sodium oxide (Na_2O) being formed as sodium is exposed to air. Self-discharge continues until the formation of the passivating layer and prevents oxidation of the electrodes further and ensures cell stability, as shown in Fig. 9. After achieving the stable potential, the cell is subjected to a discharge process through the load of 100 kΩ. The cell potential initially decreases exponentially with time and then attains a constant potential. The load voltage drops to 40%, 49% and 37% for Cell 1, Cell 2 and Cell 3, respectively, of its initial voltage after 24 h. A plateau region is observed only for Cell 2 and Cell 3 with Cell 2 giving the maximum discharge time of 16 h. Cell 3 offers a discharge time of 13 h but due to high current drain it resulted in higher energy density and power density. The cathodes used in Cell 1 and Cell 2 are intercalation-type whereas a conversion-type cathode is used in Cell 3. The insertion of sodium ions into the crystal lattice of the cathode's (MnO_2 and V_2O_5) interlayer spacing may have resulted in poor performance as compared to Cell 3.[40] The chemical reactions at the anode and cathode during discharge are given below.

$$\text{At the anode: } Na \rightarrow Na^+ + e^- \text{ (oxidation)}$$

$$\text{At the cathode of Cell 3: } 2Na^+ + 4I_2 + e^- \rightarrow NaI_2 + Na(I_3)_2$$

Conclusion

Ion–polymer complexation has brought about structural change in the solid polymer electrolyte thus affecting its thermal and electrochemical stability. Freezing of the polymer chain dynamics due to enhanced crystalline phase upon doping has influenced the ionic conductivity. The dominance of anions over cations in ion transport as the result of $Na^+\cdots O{=}C$ and $Na^+\cdots O{-}C$ interactions has resulted in a low cation transference number. The excellent mechanical properties and thermal stability of the PCL–$NaClO_4$ film reduce the risk of short circuit. The influence of the cathode material on the overall performance of the battery was observed with the I_2 cathode providing the highest discharge current over the MnO_2 and V_2O_5 cathode materials. Choosing a polymer host by considering only T_g to get desirable ionic conductivity and high cation transference number is not an effective strategy. An additional aid of computational techniques is necessary to achieve the desirable properties in solid polymer electrolytes.

Data availability

The data that support the findings of this study are available from the corresponding author upon reasonable request.

Conflicts of interest

There are no conflicts to declare.

Acknowledgements

One of the authors, Supriya K. Shetty, acknowledges the financial assistance from the Manipal Academy of Higher Education in the form of a Dr TMA Pai Scholarship and SAIF, IIT Madras for extending the DSC facility. Mr Pradeep Nayak acknowledges the financial assistance from University Grants Commission (UGC), New Delhi, Government of India in the form of a Senior Research Fellowship (SRF) with sanction number UGC-Ref. No. 1237/(CSIR-UGC NET DEC. 2017) dated 21-01-2019.

References

1 F. Bella, F. Colò, J. R. Nair and C. Gerbaldi, Photopolymer Electrolytes for Sustainable, Upscalable, Safe, and Ambient-Temperature Sodium-Ion Secondary Batteries, *ChemSusChem*, 2015, **8**(21), 3668–3676, DOI: 10.1002/cssc.201500873.

2 F. Chen, S. Cheng, J.-B. Liu, S. Li, W. Ouyang and B. Liu, Insights into the Electrochemical Stability and Lithium Conductivity of Li_4MS_4 (M = Si, Ge, and Sn), *ACS Appl. Mater. Interfaces*, 2021, **13**(19), 22438–22447, DOI: 10.1021/acsami.1c03227.

3 F. Gebert, J. Knott, R. Gorkin III, S. Chou and S. Dou, Polymer Electrolytes for Sodium-Ion Batteries, *Energy Storage Mater.*, 2021, **36**, 10–30, DOI: 10.1016/j.ensm.2020.11.030.

4 H. Tokuda, S. Tabata, A. B. H. Susan, Md., K. Hayamizu and M. Watanabe, Design of Polymer Electrolytes Based on a Lithium Salt of a Weakly Coordinating Anion to Realize High Ionic Conductivity with Fast Charge-Transfer Reaction, *J. Phys. Chem. B*, 2004, **108**(32), 11995–12002, DOI: 10.1021/jp048646r.

5 E. Quartarone and P. Mustarelli, Electrolytes for Solid-State Lithium Rechargeable Batteries: Recent Advances and Perspectives, *Chem. Soc. Rev.*, 2011, **40**(5), 2525–2540, DOI: 10.1039/C0CS00081G.

6 H. J. Woo, S. R. Majid and A. K. Arof, Conduction and Thermal Properties of a Proton Conducting Polymer Electrolyte Based on Poly (ε-Caprolactone), *Solid State Ionics*, 2011, **199–200**, 14–20, DOI: 10.1016/j.ssi.2011.07.007.

7 A. Wang, D. Pei, Z. Liu, S. Huang, G. Cao, H. Jin and S. Hou, Exploring High Li^+ Transference Number Solid-State Electrolytes Based on a Poly(ε-Caprolactone) Polymer Matrix with Efficient Lithium Salt Dissociation for Applications in Lithium-Metal Batteries, *ACS Appl. Energy Mater.*, 2023, **6**(15), 8221–8228, DOI: 10.1021/acsaem.3c01341.

8 M. Ravi, S.-H. Song, K.-M. Gu, J.-N. Tang and Z.-Y. Zhang, Effect of Lithium Thiocyanate Addition on the Structural and Electrical Properties of Biodegradable Poly(ε-Caprolactone) Polymer Films, *Ionics*, 2015, **21**(8), 2171–2183, DOI: 10.1007/s11581-015-1384-4.

9 D. M. Pesko, M. A. Webb, Y. Jung, Q. Zheng, T. F. I. Miller, G. W. Coates and N. P. Balsara, Universal Relationship between Conductivity and Solvation-Site Connectivity in Ether-Based Polymer Electrolytes, *Macromolecules*, 2016, **49**(14), 5244–5255, DOI: 10.1021/acs.macromol.6b00851.

10 A. International, *ASTM D882-12, Standard Test Method for Tensile Properties of Thin Plastic Sheeting*, ASTM International, 2012.

11 M. Biswas, J. A. Libera, S. B. Darling and J. W. Elam, Polycaprolactone: A Promising Addition to the Sequential Infiltration Synthesis Polymer Family Identified through In Situ Infrared Spectroscopy, *ACS Appl. Polym. Mater.*, 2020, **2**(12), 5501–5510, DOI: 10.1021/acsapm.0c00855.

12 M. Ravi, S.-H. Song, K.-M. Gu, J.-N. Tang and Z.-Y. Zhang, Effect of Lithium Thiocyanate Addition on the Structural and Electrical Properties of Biodegradable Poly(ε-Caprolactone) Polymer Films, *Ionics*, 2015, **21**(8), 2171–2183, DOI: 10.1007/s11581-015-1384-4.

13 I.-D. Wu and F.-C. Chang, Determination of the Interaction within Polyester-Based Solid Polymer Electrolyte Using FTIR Spectroscopy, *Polymer*, 2007, **48**(4), 989–996, DOI: 10.1016/j.polymer.2006.12.045.

14 M. F. Shukur and M. F. Z. Kadir, Electrical and Transport Properties of NH_4Br-Doped Cornstarch-Based Solid Biopolymer Electrolyte, *Ionics*, 2015, **21**(1), 111–124, DOI: 10.1007/s11581-014-1157-5.

15 M. K. Joshi, A. P. Tiwari, H. R. Pant, B. K. Shrestha, H. J. Kim, C. H. Park and C. S. Kim, In Situ Generation of Cellulose Nanocrystals in Polycaprolactone Nanofibers: Effects on Crystallinity, Mechanical Strength, Biocompatibility, and Biomimetic Mineralization, *ACS Appl. Mater. Interfaces*, 2015, **7**(35), 19672–19683, DOI: 10.1021/acsami.5b04682.

16 L. H. Sim, S. N. Gan, C. H. Chan and R. Yahya, ATR-FTIR Studies on Ion Interaction of Lithium Perchlorate in Polyacrylate/Poly(Ethylene Oxide) Blends, *Spectrochim. Acta, Part A*, 2010, **76**(3), 287–292, DOI: 10.1016/j.saa.2009.09.031.

17 E.-C. Chen and T.-M. Wu, Isothermal Crystallization Kinetics and Thermal Behavior of Poly(ε-Caprolactone)/Multi-Walled Carbon Nanotube Composites, *Polym. Degrad. Stab.*, 2007, **92**(6), 1009–1015, DOI: 10.1016/j.polymdegradstab.2007.02.019.

18 C. Baptista, A. Azagury, H. Shin, C. M. Baker, E. Ly, R. Lee and E. Mathiowitz, The Effect of Temperature and Pressure on Polycaprolactone Morphology, *Polymer*, 2020, **191**, 122227, DOI: 10.1016/j.polymer.2020.122227.

19 M. Saito, H. Ikuta, Y. Uchimoto, M. Wakihara, S. Yokoyama, T. Yabe and M. Yamamoto, Interaction between the Lewis Acid Group of a Borate Ester and Various Anion Species in a Polymer Electrolyte Containing Mg Salt, *J. Phys. Chem. B*, 2003, **107**(42), 11608–11614, DOI: 10.1021/jp034040b.

20 D. T. Hallinan and N. P. Balsara, Polymer Electrolytes, *Annu. Rev. Mater. Res.*, 2013, **43**(1), 503–525, DOI: 10.1146/annurev-matsci-071312-121705.

21 Mikrajuddin, F. G. Shi, T. G. Nieh and K. Okuyama, Electrical Conduction in Solid Polymer Electrolytes: Temperature Dependence Mechanism, *Microelectron. J.*, 2000, **31**(4), 261–265, DOI: 10.1016/S0026-2692(99)00138-X.

22 G. Sivalingam and G. Madras, Thermal Degradation of Binary Physical Mixtures and Copolymers of Poly(ε-Caprolactone), Poly(d, l-Lactide), Poly(Glycolide), *Polym. Degrad. Stab.*, 2004, **84**(3), 393–398, DOI: 10.1016/j.polymdegradstab.2003.12.008.

23 S. K. Shetty, Ismayil, I. S. Mohd Noor, S. N. Yethadka and P. Nayak, Deciphering the Effect of Microstructural Modification in Sodium Alginate-Based Solid Polymer Electrolyte by Unlike Anions, *ACS Omega*, 2023, **8**(46), 43632–43643, DOI: 10.1021/acsomega.3c05094.

24 K. Funke, Jump Relaxation in Solid Electrolytes, *Prog. Solid State Chem.*, 1993, **22**(2), 111–195, DOI: 10.1016/0079-6786(93)90002-9.

25 S. R. Elliott, The Mechanism for a.c. Conduction in Chalcogenide Semiconductors: Electronic or Atomic?, *Philos. Mag. B*, 1979, **40**(6), 507–511, DOI: 10.1080/01418637908226775.

26 I. G. Austin and N. F. Mott, Polarons in Crystalline and Non-Crystalline Materials, *Adv. Phys.*, 1969, **18**(71), 41–102, DOI: 10.1080/00018736900101267.

27 B. Natesan, N. K. Karan and R. S. Katiyar, Ion Relaxation Dynamics and Nearly Constant Loss Behavior in Polymer Electrolyte, *Phys. Rev. E: Stat., Nonlinear, Soft Matter Phys.*, 2006, **74**(4), 042801, DOI: 10.1103/PhysRevE.74.042801.

28 N. K. Karan, D. K. Pradhan, R. Thomas, B. Natesan and R. S. Katiyar, Solid Polymer Electrolytes Based on Polyethylene Oxide and Lithium Trifluoro- Methane Sulfonate (PEO–$LiCF_3SO_3$): Ionic Conductivity and Dielectric Relaxation, *Solid State Ionics*, 2008, **179**(19), 689–696, DOI: 10.1016/j.ssi.2008.04.034.

29 B. Natesan, N. K. Karan and R. S. Katiyar, Ion Relaxation Dynamics and Nearly Constant Loss Behavior in Polymer Electrolyte, *Phys. Rev. E: Stat., Nonlinear, Soft Matter Phys.*, 2006, **74**(4), 042801, DOI: 10.1103/PhysRevE.74.042801.

30 T. Dam, S. S. Jena and D. K. Pradhan, Coupled Ion Conduction Mechanism and Dielectric Relaxation Phenomenon in PEO20–$LiCF_3SO_3$-Based Ion Conducting Polymer Nanocomposite Electrolytes, *J. Phys. Chem. C*, 2018, **122**(8), 4133–4143, DOI: 10.1021/acs.jpcc.7b11112.

31 W. K. Lee, J. F. Liu and A. S. Nowick, Limiting Behavior of Ac Conductivity in Ionically Conducting Crystals and Glasses: A New Universality, *Phys. Rev. Lett.*, 1991, **67**(12), 1559–1561, DOI: 10.1103/PhysRevLett.67.1559.

32 A. M. Christie, S. J. Lilley, E. Staunton, Y. G. Andreev and P. G. Bruce, Increasing the Conductivity of Crystalline Polymer Electrolytes, *Nature*, 2005, **433**(7021), 50–53, DOI: 10.1038/nature03186.

33 D. Bresser, S. Lyonnard, C. Iojoiu, L. Picard and S. Passerini, Decoupling Segmental Relaxation and Ionic Conductivity for Lithium-Ion Polymer Electrolytes, *Mol. Syst. Des. Eng.*, 2019, **4**(4), 779–792, DOI: 10.1039/C9ME00038K.

34 S. B. Aziz, T. J. Woo, M. F. Z. Kadir and H. M. Ahmed, A Conceptual Review on Polymer Electrolytes and Ion Transport Models, *J. Sci.: Adv. Mater. Devices*, 2018, **3**(1), 1–17, DOI: 10.1016/j.jsamd.2018.01.002.

35 H. Zhang, C. Li, M. Piszcz, E. Coya, T. Rojo, L. M. Rodriguez-Martinez, M. Armand and Z. Zhou, Single Lithium-Ion Conducting Solid Polymer Electrolytes: Advances and Perspectives, *Chem. Soc. Rev.*, 2017, **46**(3), 797–815, DOI: 10.1039/C6CS00491A.

36 S. Chandra, S. K. Tolpadi and S. A. Hashmi, Transient Ionic Current Measurement of Ionic Mobilities in a Few Proton Conductors, *Solid State Ionics*, 1988, **28–30**, 651–655, DOI: 10.1016/S0167-2738(88)80119-X.

37 K. M. Abraham, How Comparable Are Sodium-Ion Batteries to Lithium-Ion Counterparts?, *ACS Energy Lett.*, 2020, **5**(11), 3544–3547, DOI: 10.1021/acsenergylett.0c02181.

38 K. Mishra, T. Arif, R. Kumar and D. Kumar, Effect of Al_2O_3 Nanoparticles on Ionic Conductivity of PVdF-HFP/PMMA Blend-Based Na^+-Ion Conducting Nanocomposite Gel Polymer Electrolyte, *J. Solid State Electrochem.*, 2019, **23**(8), 2401–2409, DOI: 10.1007/s10008-019-04348-9.

39 J. Zhang, J. Zhao, L. Yue, Q. Wang, J. Chai, Z. Liu, X. Zhou, H. Li, Y. Guo, G. Cui and L. Chen, Safety-Reinforced Poly(Propylene Carbonate)-Based All-Solid-State Polymer Electrolyte for Ambient-Temperature Solid Polymer Lithium Batteries, *Adv. Energy Mater.*, 2015, **5**(24), 1501082, DOI: 10.1002/aenm.201501082.

40 P. Nayak, I. Ismayil, S. K. Shetty, Y. N. Sudhakar and S. Hegde, Unleashing the Potential of Eco-Friendly Chitosan: Methylcellulose Polyblend Electrolytes via Magnesium Acetate Doping for Solid State Batteries, *J. Energy Storage*, 2023, **72**, 108503, DOI: 10.1016/j.est.2023.108503.